# Spatial Disaggregation of Particulate Matter Emission Inventory in the Metropolitan Area of Aburrá Valley for Air Quality Modelling

Santiago Lopez-Restrepo[a,d,*], Andres Yarce[a,c,d], Nicolás Pinel[b,c], O. L. Quintero[a], Arjo Segers[e] and A. W. Heemink[d]

[a]Mathematical Modelling Research Group, Universidad EAFIT. Medellín, Colombia
[b]Department of Biological Sciences, Universidad EAFIT. Medellín, Colombia
[c]Biodiversity, Evolution and Conservation Research Group, Universidad EAFIT. Medellín, Colombia
[d]Department of Applied Mathematics, TU Delft. Delft, The Netherlands
[e]Department of Climate, Air and Sustainability, TNO. Utrecht, The Netherlands

ARTICLE INFO

*Keywords*:
Air quality modelling
Top-down emission inventory
Chemical transport model
Particulate Matter
Local emissions inventory
LOTOS-EUROS

ABSTRACT

In this paper a local emission inventory for $PM_{10}$ and $PM_{2.5}$ is presented that has been developed using a top-down spatial disaggregation of the official emission inventory for the Metropolitan Area of the Aburrá Valley in Colombia. The local emission inventory was evaluated using the LOTOS-EUROS Chemical Transport Model in a high-resolution simulation, and compared with the global emission inventory EDGAR. A detailed analysis of the model using the local emission inventory was performed. The results showed a considerable improvement in model performance when the local emission inventory was used in comparison to the global emission inventory.

## 1. Introduction

Air pollution has become one of the most important concerns of local authorities of growing cities in Latin American (Kumar, Jiménez, Belalcázar and Rojas, 2016). Emissions from urban agglomerations are major sources of regional and global atmospheric pollution (Green and Sánchez, 2012). An example of this is the Aburrá Valley that constitutes the second most populous metropolitan area in Colombia. It is composed of the city of Medellín and its neighboring municipalities. Within the Aburrá Valley, air quality conditions deteriorate with the overpass of the 1 Intertropical Convergence Zone (March-April, and with lower intensity in October-November). During the overpass, the atmospheric boundary layer stays often below the rim of the canyon, trapping the pollutants within the valley (Jiménez, 2016).

Due to the large stress on human health induced by this air pollution, efforts have been made to monitor, reduce, and prevent episodes in which concentrations of pollutants reach hazard levels. Before measures for reducing air pollution can be implemented it is important to know the actual concentration levels and how these evolve in time over the area of interest. This could be done using a Chemical Transport Model (CTM) to simulate concentrations of trace gasses and particulate matter (Thunis, Miranda, Baldasano, Blond, Douros, Graff, Janssen, Juda-Rezler, Karvosenoja, Maffeis, Martilli, Rasoloharimahefa, Real, Viaene, Volta and White, 2016; Lateb, Meroney, Yataghene, Fellouah, Saleh and Boufadel, 2016).

An early study on atmospheric pollution in Colombia used the WRF-CHEM model (Weather Research and Forecasting with Chemistry) to simulate the concentrations of $PM_{10}$ over the Bogotá metropolitan area (Kumar et al., 2016). The EDGAR (Emissions Database for Global Atmospheric Research) global emission inventory was used as input. The simulations underestimated the $PM_{10}$ concentrations by an order of magnitude compared to observations. The WRF-CHEM model has also been applied to study the behavior of $O_3$ over the medium-size, mountainous city of Manizales (González, Ynoue, Vara-Vela, Rojas and Aristizábal, 2018). By using high-resolution simulations (1x1 km), the study compared the performance of the model when using either the EDGAR emission inventory or a high-resolution emission inventory previously developed (Gonzalez, Gomez, Rojas, Acevedo and Aristizabal, 2017). This study showed a significant improvement of the model performance when using the high-resolution emission inventory.

*Corresponding author
slopezr2@eafit.edu.co,s.lopezrestrepo@tudelft.nl (S. Lopez-Restrepo)
ORCID(s): 0000-0002-7637-1575 (S. Lopez-Restrepo); 0000-0003-1441-2367 (A. Yarce); 0000-0003-1304-3096 (N. Pinel); 0000-0002-8697-4361 (O.L. Quintero); 0000-0002-1319-0195 (A. Segers); 0000-0001-8559-9566 (A.W. Heemink)

For the city of Medellín, a similar under estimation of $PM_{2.5}$ and $PM_{10}$ concentrations has been observed for simulations with the LOTOS-EUROS CTM (Lopez-Restrepo, Yarce, Pinel, Quintero, Segers and Heemink, 2020), which also used the global EDGAR inventory as input. Data assimilation was used to adjust the emissions, and due to the persistent low bias the best performance was obtained by strongly increasing the emissions over the entire domain. Despite repeated studies showing that the EDGAR inventory has its limitations for application over Colombian (Gonzalez et al., 2017; Pachón, Galvis, Lombana, Carmona, Fajardo, Rincón, Meneses, Chaparro, Nedbor-Gross and Henderson, 2018; Nedbor-Gross, Henderson, Pérez-Peña and Pachón, 2018), this database is still the only one available that includes all species necessary for air quality simulations over a large region of the northeast Andes domain.

In this paper, a disaggregation methodology is proposed to create a local map of particulate matter (PM) emissions that is suitable for modelling purposes. The emissions are based on the current official emission inventory for the Metropolitan Area of the Aburrá Valley. The new emission inventory is compared with the global emission inventory EDGAR v4.3 (Crippa, Guizzardi, Muntean, Schaaf, Dentener, van Aardenne, Monni, Doering, Olivier, Pagliari and Janssens-Maenhout, 2018), and used in simulations with the LOTOS-EUROS model. The simulated particulate matter concentrations are compared with observations from surface stations from a local air quality network.

The paper is organized as follows. Section 2 presents the relevant information regarding the emission data and how the new emission inventory was built. The simulation model, observations and methodology used to validate the simulations are also presented. Section 3 shows the local emission inventory and a comparison with the EDGAR v4.3 emissions. In this section the simulated PM concentrations are evaluated for two different periods using both the new local inventory as well as the original global inventory. Section 4 summarizes the main conclusions and provides an outlook for future research.

## 2. Materials and methods

### 2.1. Local emission inventories

The base of the new emission map is formed by an on-road vehicular and industrial point-source inventory developed by the Área Metropolitana del Vallé de Aburrá (AMVA) in cooperation with the Universidad Pontificia Bolivariana located in Medellín, Colombia (UPB and AMVA, 2017)[1]. The inventory was initially created for 2015 and updated in 2016. The database covers the 10 municipalities that together constitute the Metropolitan Area of the Aburrá Valley shown in Figure 5. The AMVA emission inventory provides a complete set of emitted trace gases such as carbon monoxide (CO), nitrogen oxides ($NO_x$), sulpheric oxides ($SO_x$), and volotile organic compounds (VOC's), as well as particulate matter with diameters less than 2.5 $\mu$m ($PM_{2.5}$) or less than 10 $\mu$m ($PM_{10}$). The particulate matter emissions form the largest contribution to the air quality deterioration in the Valley (Hoyos, Herrera-Mejía, Roldán-Henao and Isaza, 2019), and these are therefore the focus of this study. The AMVA inventory followed a bottom-up methodology, combining activity data (traffic intensities, industrial production) with emission factors. Only traffic and industrial point sources are considered, neither household or commercial sources are taken into account.

#### *2.1.1. Traffic emissions*

The data for the traffic emissions in the AMVA inventory originates from the mobility offices at all ten municipalities of the Valley. Five vehicle categories are distinguished: passenger cars, taxis, buses, trucks (including tractor and tipper trucks), and motorcycles (subdivided in two groups with different engine capacity and type of motor, namely 2-stroke motors < 100 cc; and 4-stroke motors (cc<100,100<cc<300,300<cc)). The total number of registered vehicles in the metropolitan area for 2016 was 1.3 million. Figure 1 shows the total number of vehicles by category, and the corresponding type of fuel used. Despite motorcycles being the dominant category, their overall contribution to emissions is lower than diesel-fueled trucks.

The total emissions for $PM_{10}$ and $PM_{2.5}$ by vehicle category for the year 2016 are shown in Figure 2 (a). The total yearly contribution of $PM_{2.5}$ is higher than that of PM10. While trucks dominate in the emissions of $PM_{2.5}$, passenger cars are the main source of vehicular $PM_{10}$.

#### *2.1.2. Point source emissions*

Data for industrial point-source emissions had been collected from large and medium-size industrial facilities within the Aburrá Valley. Information for 12 different industrial activities was gathered from the official reporting to the environmental agency. Of these, eight economic activities that represent more than 98% of the total emissions are taken into

[1] available from https://www.metropol.gov.co/ambiental/calidad-del-aire/Documents/Inventario-de-emisiones

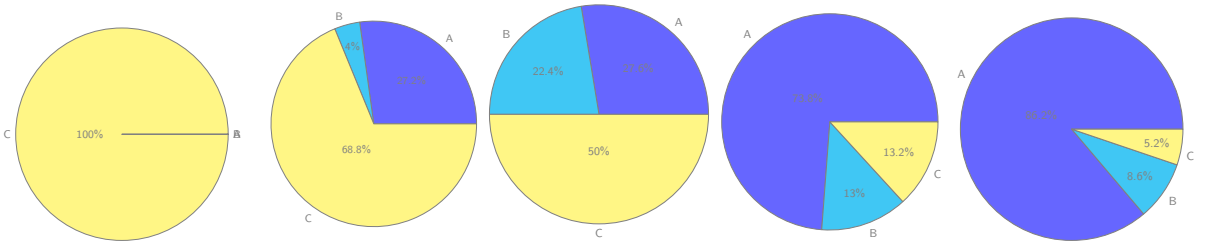


(a) Motorcycles 674.128 (b) Passengers 501.894 (c) Taxis 49.892 (d) Buses 19.942 (e) Trucks 39.864

**Figure 1:** Total number of mobile sources per category, and subdivision of mobile sources in terms of type of fuel: A - Diesel, B-Natural Gas, and C-Gasoline.

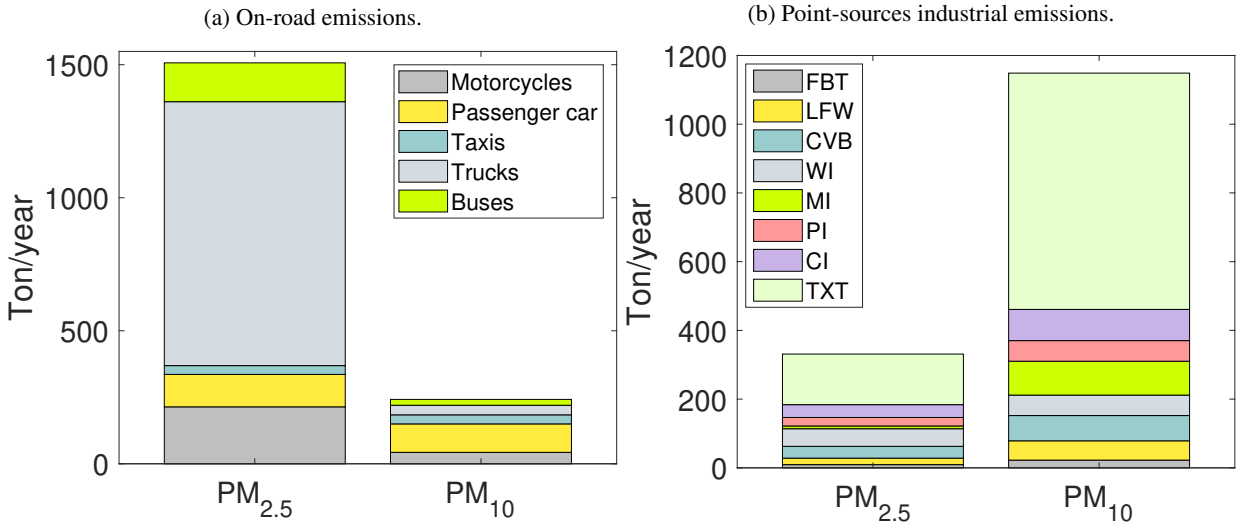


**Figure 2:** Total $PM_{10}$ and $PM_{2.5}$ emissions in the AMVA inventory for the five vehicle categories (a), and the particulate matter emissions from industrial point sources (b).

account in this study: 1) Food, Beverage and Tobacco (FBT); 2) Leather and Footwear (LFW); 3) Ceramic, Vitreous, Brick Makers, Potters, Tiles and Ceramic industries (CVB); 4) Wood industry (WdI); 5) Metallurgical industry (MI); 6) Paper Industry (PI); 7) Chemical industry (CI); and 8) Textiles (TXT). Emission factors that define the emission strength given unit of production were taken from the EPA AP-42 report (US EPA (United State Environmental Protection Agency), 1995) and applied for each industrial facility based on the reported type of fuel, type of combustion equipment, and firing configuration. The information included in the AMVA inventory covered 432 industrial facilities and 1448 emission point sources. The annual emission total for $PM_{10}$ and $PM_{2.5}$ by economic activity is shown in Figure 2(b), which was calculated from the activity level of the industry, the emission factor, but was partly also based on direct sampling campaigns. The TXT, MI, FBT and CI sectors are responsible for the majority of industrial emissions, with TXT contributing the largest amount. The Wood Industry is the second largest producer of $PM_{2.5}$ pollution, despite that the sector occupies just 2 percent of the point sources and 3 percent of all the industrial sites in the inventory.

## 2.2. Temporal disaggregation

To be able to use the AMVA emission information in a simulation model, it is necessary to expand it with a temporal profile. The temporal profile distributes a yearly total emission over seasons (months), days (work days or weekends), and hours of the day. For road-traffic emissions, a daily profile following the traffic density for a working day in the metropolitan area was taken from (UPB and AMVA, 2017). This profile has an hourly resolution, as shown in Figure 4. Industrial emissions can have a strong variability within a day, but since no detailed information is available,

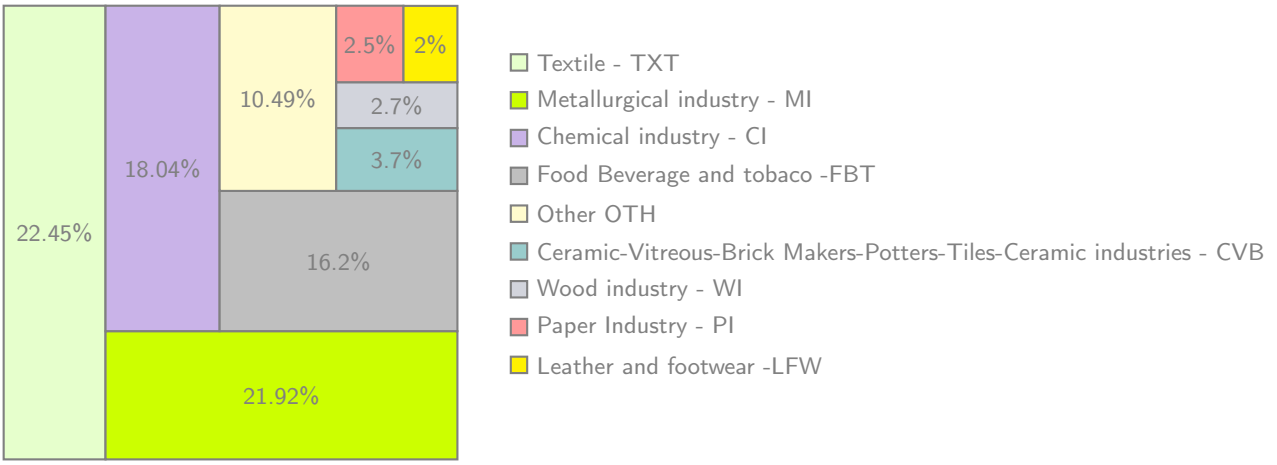


**Figure 3:** Percentage of industrial facilities per economy activities.

their temporal profile is kept constant in this study.

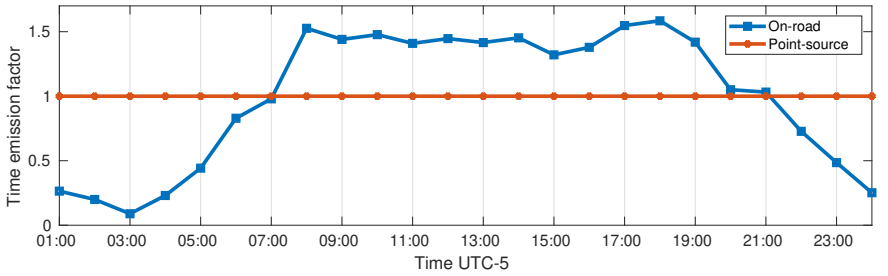


**Figure 4:** Temporal emission profiles used for traffic and industrial point source emissions.

## 2.3. Spatial disaggregation

Apart from a temporal profile, a simlation model also requires a spatial disaggregation. The result is a map of emission intensities that shows spatial differences in emission strengths; the total sum should equal the inventory data.

The AMVA inventory was disaggregated over the Metropolitan Area of the Aburrá Valley ( 76°W-75°W and 5.7°N-6.8°N ) at a resolution of $0.01° \times 0.01°$(approximately 1 km $\times$ 1 km). Dissagregation methods use variables such as land use and population density maps, traffic counts, and simplified and complete road networks to assign emissions to grid cells (Saide, Zah, Osses and Ossés de Eicker, 2009). A Dissagregation Factor (DF) can be derived from normalized weights for each cell in the domain based on specific information such as traffic intensity or road density (Saide et al., 2009; Shu and Lam Nina, 2011).

In this study, a method based on road density was implemented following (Ossés de Eicker, Zah, Triviño and Hurni, 2008). The road network map was obtained from the OpenStreetMap database (Haklay and Weber, 2008), and simplified by removing the segments classified as residential, as recommended in (Tuia, Ossés de Eicker, Zah, Osses, Zarate and Clappier, 2007; Gómez, González, Osses and Aristizábal, 2018). The simplification of the road network can reduce errors in the spatial disaggregation since normally residential roads correspond to a high portion of the road network length but carry a low percentage of vehicular traffic (Gonzalez et al., 2017). Although this method is one of the simplest disaggregation methods, it has been shown as a valuable method for high-density cities (as is the case of the Metropolitan Area of the Aburrá Valley), and in applications where detailed information about traffic intensity is not available (Tuia et al., 2007).

For each grid cell $j$, the corresponding $DF$ was calculated with (Ossés de Eicker et al., 2008):

$$DF_j = \frac{\sum_{i=0}^{I} S_{i,j}}{\sum_{j=0}^{J} \sum_{i=0}^{I} S_{i,j}} \quad (1)$$

where $S_{i,j}$ is the road segment $i$ in the grid cell $j$, $I$ is the total length of road segments in each grid cell, and $J$ is the total number of grid cells. Figure 5 shows the simplified road network map used for the on-road spatial disaggregation.

The point-source emissions were distributed on the grid using their known location, obtained from the official emissions inventory (UPB and AMVA, 2017).

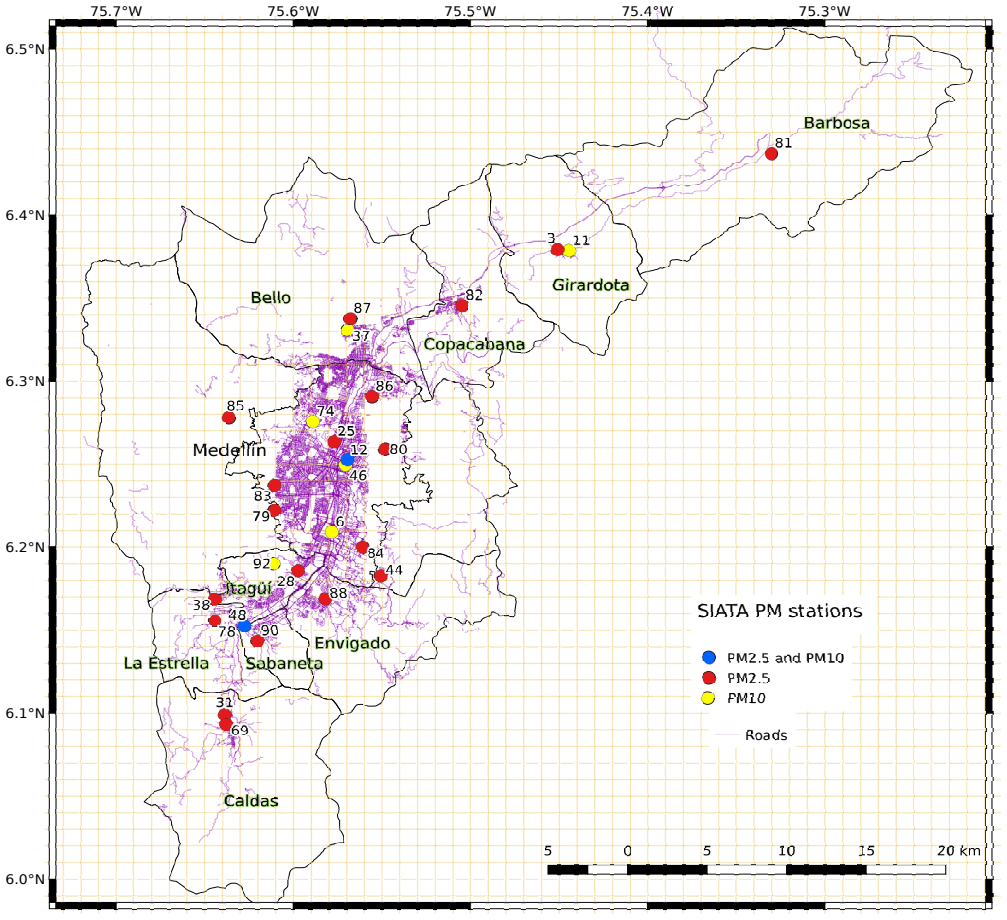


**Figure 5:** Simplified road network of the Metropolitan Area of the Aburrá Valley and SIATA particulate matter station distribution. The raster corresponds to the chosen emission grid.

## 2.4. LOTOS-EUROS model

The LOTOS-EUROS (LOng Term Ozone Simulation - EURopean Operational Smog) model is a 3D Chemical Transport Model that simulates trace gas and aerosol concentrations in the lower troposphere (Manders, Builtjes, Curier, Denier Van Der Gon, Hendriks, Jonkers, Kranenburg, Kuenen, Segers, Timmermans, Visschedijk, Kruit, Addo, Van Pul, Sauter, Van Der Swaluw, Swart, Douros, Eskes, Van Meijgaard, Van Ulft, Van Velthoven, Banzhaf, Mues, Stern, Fu, Lu, Heemink, Van Velzen and Schaap, 2017). The simulated concentrations include ozone, particulate matter, nitrogen dioxide, heavy metals, and organic components (Sauter, der Swaluw, Manders-groot, Kruit, Segers and Eskes, 2012). The physical processes in the model include emission, advection, diffusion, chemical reactions, and

dry and wet deposition. The input to the LOTOS-EUROS model mainly consists of meteorological data, emission inventories, and surface data such as land-use and vegetation type. LOTOS-EUROS has demonstrated its capacity through a wide use in different projects around the world (Manders, Schaap and Hoogerbrugge, 2009; Curier, Timmermans, Calabretta-Jongen, Eskes, Segers, Swart and Schaap, 2012; Mues, Kuenen, Hendriks, Manders, Segers, Scholz, Hueglin, Builtjes and Schaap, 2014; Fu, Heemink, Lu, Segers, Weber and Lin, 2016; Jin, Lin, Heemink and Segers, 2018; Lopez-Restrepo et al., 2020). For a full description of the physical processes and input data could be found in Manders et al. (2017).

Two different time periods were selected to analyze the model performance using the new emission inventory. The first period covered 8-25 January 2019 which represents cases with moderate concentration that are close to the annual mean. The second period covered 25-February through 15-March which represents cases with high concentrations, related to overpass of the ITCZ. The spatial domains and the summarize of the experimental setup are presented in the Table 1 For each period, two simulations were performed using different anthropogenic emission inventories for the inntermost domain (D4): either EDGAR V4.3, or the disaggregated AMVA inventory.

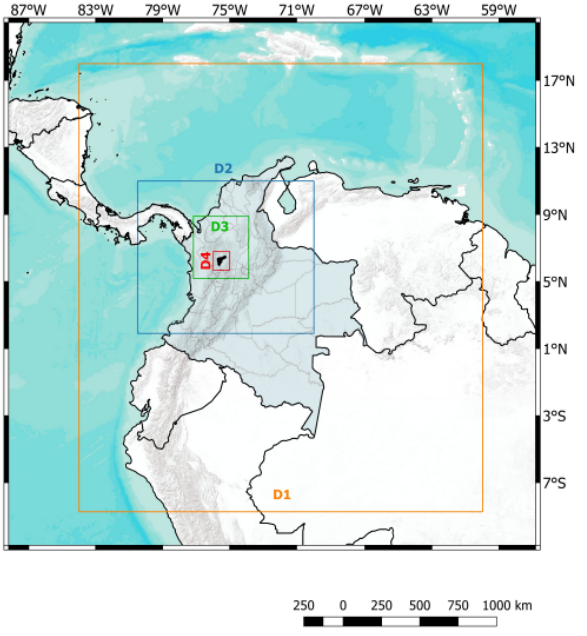


**Figure 6:** LOTOS-EUROS model nested domains for Metropolitan Area of Aburrá Valley assessment.

## 2.5. Ground based sensor network and Performance metrics for validations

The Sistema de Alerta Temprana del Valle de Aburrá (SIATA, `www.siata.gov.co`) is a sensor network that provides automatic and high-quality measurements of air pollutant concentrations in the metropolitan area of the Aburrá Valley. The observed species include $O_3$, $SO_2$, $PM_{10}$, $PM_{2.5}$ and $PM_1$. The network consist of 9 stations measuring $PM_{10}$, and 21 stations measuring $PM_{2.5}$. The distribution of the stations across the Aburrá Valley is shown in Figure 5. The $PM_{2.5}$ and $PM_{10}$ equipment consists of Met One Instruments BAM-1020 and BAM-1022 monitors using a beta ray attenuation method to measure airborne PM concentration levels (Hoyos et al., 2019). In this study, the $PM_{10}$ and $PM_{2.5}$ stations selected for validation should have at least 70% data coverage for the periods of interest.

Three different metrics are used to compare observations from ground stations with simulations of the LOTOS-EUROS model.

- The *mean fractional bias* (MFB) normalizes the bias between observation and simulations using division by the

| Domain | Longitude | Latitude | Cell size | Approx. resolution |
|---|---|---|---|---|
| **D1** | 84°W-60°W | 8.5°S-18°N | 0.27° x 0.27° | 28 km |
| **D2** | 80.5°W-70°W | 2°N-11°N | 0.09° x 0.09° | 9 km |
| **D3** | 77.2°W-73.9°W | 5.2°N-8.9°N | 0.03° x 0.03° | 3 km |
| **D4** | 76°W-75°W | 5.7°N-6.8°N | 0.01° x 0.01° | 1 km |
| **Meteorology** | ECMWF<br>D1 = Temp. Res.: 3h; Spat. Res.: 0.14° x 0.14°<br>D2-4 = Temp. Res.: 3h; Spat. Res.: 0.07° x 0.07° | | | |
| **Initial and boundary conditions** | LOTOS-EUROS. (D3). Temp.res:1h<br>Spat.Res: 0.03° x 0.03° | | | |
| **Biogenic emissions** | MEGAN. Spat. Res.: 10 km x 10 km | | | |
| **Fire emissions** | GFAS. Spat. Res.: 10 km x 10 km | | | |
| **Landuse** | GLC2000. Spat. Res.: 1km x 1km | | | |
| **Orography** | GMTED2010. Spat. Res.: 0.002°x0.002° | | | |

**Table 1**
Nested domain specifications and model inputs for LOTOS-EUROS simulations. Simulation results from D4 were used to evaluated the impact of the disaggregated emissions inventory on model performance.

average of the model and observation before taking the sample mean (Boylan and Russell, 2006):

$$\mathrm{MFB} = \frac{2}{M}\sum_{i=1}^{M}\frac{\left(y^{LE}\right)_i - y_i^o}{\left(y^{LE}\right)_i + y_i^o} \tag{2}$$

where $M$ is the number of observations, $y_i^{LE}$ is the model simulation output, and $y_i^o$ is the observation.

- The *root mean square error* (RMSE) represents the sample standard deviation of the differences between predicted values and observed values (Zhang, Roussel, Boniface, Cuong Ha, Frappart, Darrozes, Baup and Calvet, 2017):

$$\mathrm{RMSE} = \sqrt{\frac{1}{M}\sum_{i=1}^{M}\left(\left(y^{LE}\right)_i - y_i^o\right)^2} \tag{3}$$

The RMSE penalizes a high variance as it gives errors with larger absolute values more weight than errors with smaller absolute values (Chai and Draxler, 2014).

- The last metric used is the *correlation factor* (CF), which shows how the values from one data set (simulations) relate to the value of a second data set (observations). The correlation coefficient is calculated following:

$$\mathrm{CF} = \frac{\sum_{i=1}^{M}\left((y^{LE})_i - \overline{(y^{LE})}(y_i^o - \overline{y^o})\right)}{\sqrt{\sum_{i=1}^{M}\left((y^{LE})_i - \overline{(y^{LE})}\right)^2}\sqrt{\sum_{i=1}^{M}(y_i^o - \overline{y^o})^2}} \tag{4}$$

where the overline denotes a sample mean over the $M$ elements.

## 3. Results

Using the disaggregation methodology described in Section 2.3 with the data presented in Section 2.1, a local emission inventory suitable for model simulation was obtained. To carry out a complete evaluation of the new AMVA emission inventory, different types of comparisons were made. First, a comparison between the total emissions and the spatial distribution in the AMVA and EDGAR V4.3 inventories is made in sections 3.1 and 3.2. This comparison evaluates the spatial representativeness of the new emissions inventory and compares it to the global inventory. Second,

an evaluation of the LOTOS-EUROS model using both emission inventories as input is made in sections 3.3 and 3.4. A comparison is made between the simulated particulate matter concentrations and the observations from the SIATA network. Evaluating the modeled concentrations, it was possible to assess the performance of the new emission inventory and to identify the most important improvements when this data is used instead of the global inventory.

### 3.1. Comparison of global and local traffic emissions

Traffic emissions represent the largest urban source of $PM_{2.5}$ Zavala, Barrera, Morante and Molina (2013); Premalatha Kanikannan and Duraiswamy (2014); Ferm and Sjöberg (2015). For the considered domain, about 80% of the total $PM_{2.5}$ emissions can be attributed to traffic, as shown in Figure 2. Figure 7 shows a comparison between the local AMVA emissions inventory and the global emission inventory EDGAR V4.3 for traffic $PM_{2.5}$ emissions. For EDGAR V4.3, the map shows section "1A3b" that corresponds with road transportation (Crippa et al., 2018).

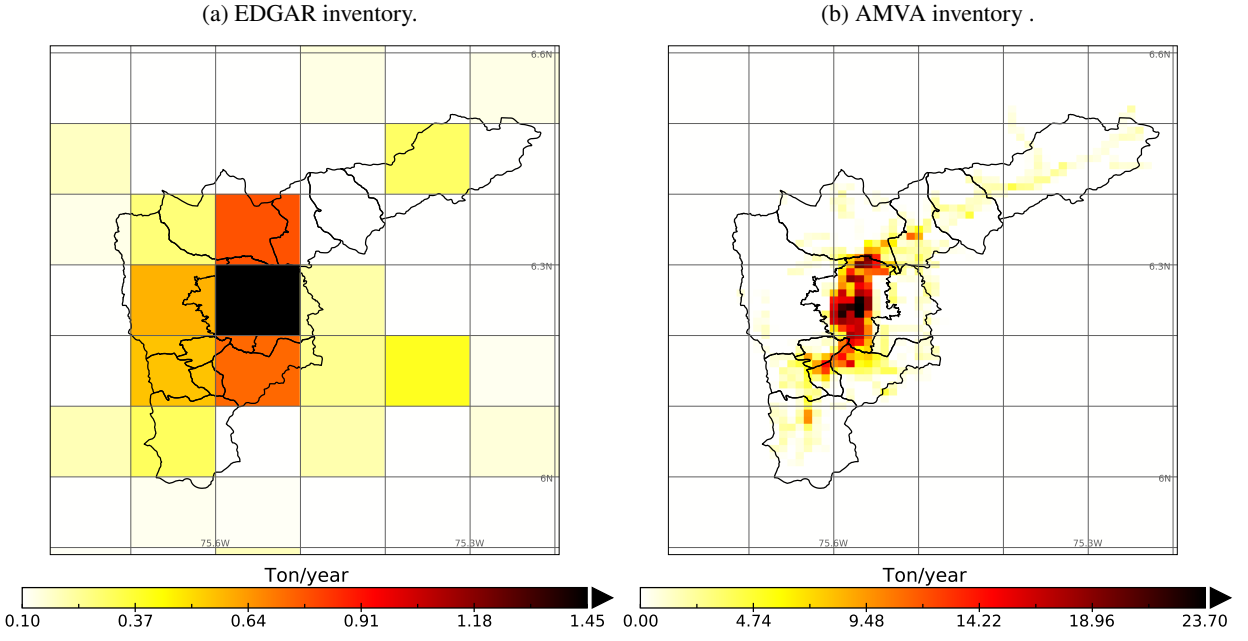


**Figure 7:** $PM_{2.5}$ on-road annual emissions in (a) EDGAR v4.3 and (b) AMVA inventory.

The AMVA inventory has a much higher spatial resolution (1x1 km) than EDGAR (10x10 km). Although this does not necessarily means an improvement in accuracy, a higher resolution does allow a more detailed spatial representation of emissions. The spatial resolution is especially important for the Aburrá Valley since it has a complicated topography (a narrow and deep valley) with emissions concentrated in a rather small area.

In the low resolution emission map of EDGAR, on-road emissions are assigned to locations in the eastern part of the city of Medellín (located in the center of the valley, see Figure 5) and to the grid cells north and south of it, which are mainly rural zones. This coarse representation does not allow to differentiate the main road corridors or the areas characterized by high vehicular flow in the city. González et al. (2018) observed a similar situation for the Colombian city of Manizales.

The disaggregated AMVA inventory provides a more detailed representation of the city's traffic network. In this inventory, it was possible to differentiate the main vehicular artery that traverses the valley from south to north-east. The largest share of emissions is concentrated in the center of the city of Medellín (largest urban hub in the metropolitan area), and along its Southern borders with Envigado, Sabaneta, and Itagui (see Figure 5), a location characterized by high vehicular traffic and frequent congestion. The use of a simplified road map instead of the complete map avoided over-estimation of traffic emission in the residential areas located on the slopes of the valley, which are characterized by high road density but low vehicle flow.

In terms of total emissions for the region, the EDGAR inventory estimates a total $PM_{2.5}$ emission from road traffic that is approximately 18 times lower than the estimate in the by AMVA inventory. The lower total suggest that the

EDGAR inventory might underestimate emissions from the transportation sector in midsize cities compared to their upstream and local emissions inventories (Gonzalez et al., 2017).

## 3.2. Comparison of industrial point-source emissions

Figure 8 shows a comparison between the $PM_{10}$ industrial point-source emissions from the disaggregated AMVA inventory, and EDGAR v4.3 (combustion for manufacturing 1A2, chemical processes 2B, food and paper 2D, and iron and steel production (Crippa et al., 2018)).

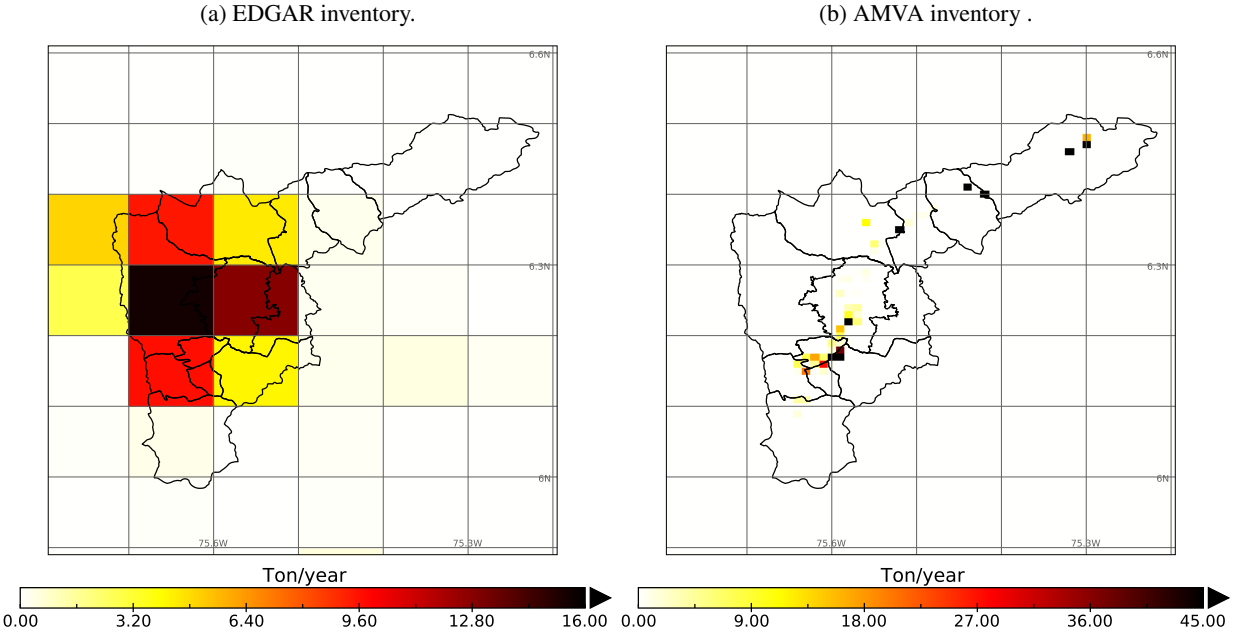


**Figure 8:** $PM_{10}$ industrial point-source emissions in (a) EDGAR v4.3 and (b) AMVA inventory.

Industrial sources are the major contributors to $PM_{10}$ emissions as shown in Figure 2. The Metropolitan Area of the Aburrá Valley has a well-defined distribution of industrial facilities, located mainly in the center and the Southwestern part of the city of Medellín and the municipality of Itagüí. The north of the valley hosts mainly quarries and mines for the extraction of construction material. The high resolution of the AMVA inventory has the advantage of being able to accurately represent the location of the industrial sources, where the EDGAR resolutions only allow a very crude spatial assignment. In the global inventory, the main source of industrial emissions appears on the western flank of the Valley, which is actually mainly a residential or even rural area.

In terms of total $PM_{10}$ emissions, the EDGAR estimate is very similar to the values estimated by AMVA. Although EDGAR is known to overestimate industrial emissions of gases such as NVMOC, CO, and $NO_x$ in the Colombian city of Manizales (Gonzalez et al., 2017; González et al., 2018), this seems not the case for the the Aburrá Valley. For $PM_{2.5}$, EDGAR estimate exceeds the AMVA with a factor 10.

## 3.3. Simulated concentrations

The difference in representation of PM emissions between the high-resolution local inventory and the coarse-resolution global emission has been evaluated using simulations with the LOTOS-EUROS CTM. Two simulations were carried out using different inventories for $PM_{2.5}$ and $PM_{10}$, while the remaining species (e.g., $NO_x$, CO, $SO_x$), were taken from EDGAR v4.3 in both cases. In the first simulation the disaggregated high-resolution local emission inventory was used as described in Subsection 2.3 (hereafter referred to as the LE-AMVA simulation); in the second simulation, the global emission inventory EDGAR v4.3 was used (LE-EDGAR simulation).

Time series of simulated concentrations are shown in figures 9 and 10 for four stations each. The diurnal cycles are shown in figures 11 and 12 for the same stations. The selected stations are located in the north (stations 3, and 11 ), center (stations 25, 28, 6, and 74), and south of the valley (stations 90, and 48) as marked in Figure 5. The stations are representative for residential areas (stations 3,11, 74, and 90), highways and areas of high vehicular flow (stations

6, 25, and 28), or an industrial area (48). Figures 14 and 13 show a comparison between the MFB, RMSE, and CF measures for all stations with data available.

(a) Station 3 Normal Concentration Period.

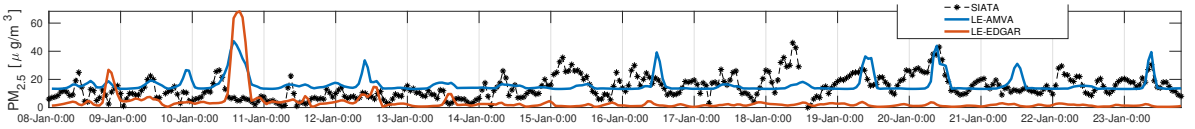


(b) Station 25 Normal Concentration Period.

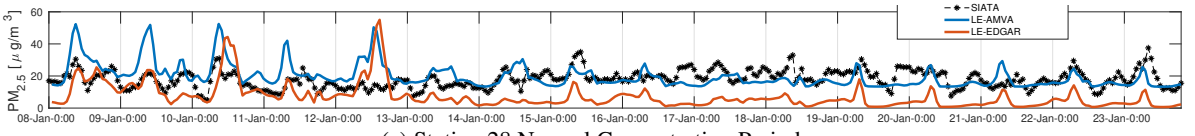


(c) Station 28 Normal Concentration Period.

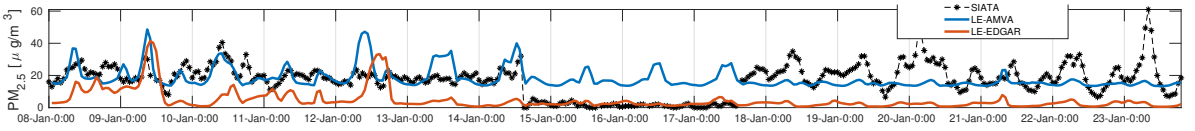


(d) Station 90 Normal Concentration Period.

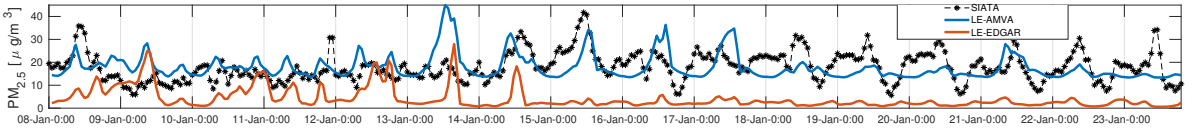


(e) Station 3 High Concentration Period.

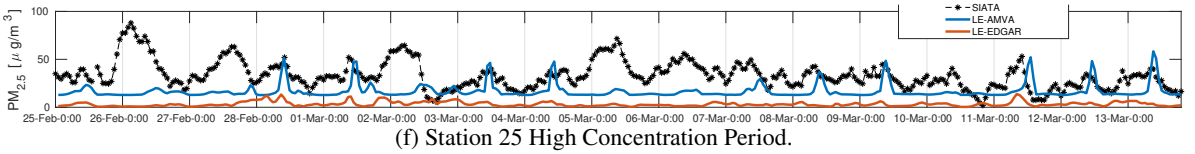


(f) Station 25 High Concentration Period.

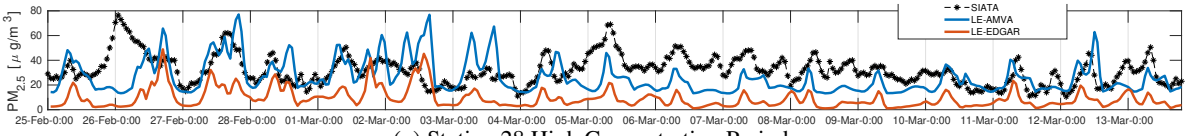


(g) Station 28 High Concentration Period.

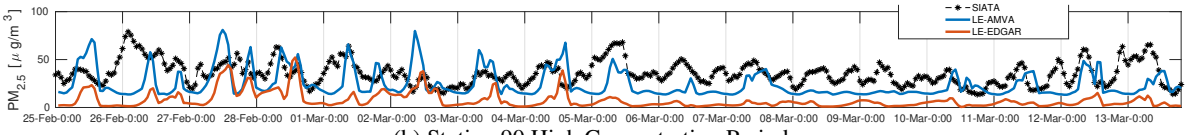


(h) Station 90 High Concentration Period.

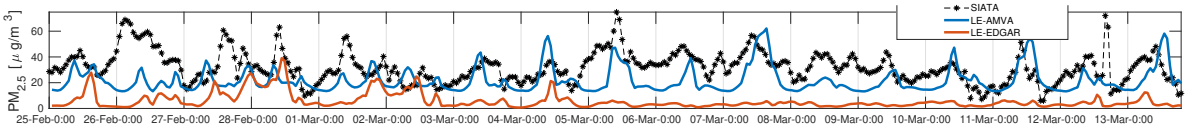


**Figure 9:** Comparison of LE-AMVA and LE-EDGAR $PM_{2.5}$ concentration against SIATA observations for both concentrations period. The time axis corresponds with the local time zone UTC-5.

In general, the model performance improved significantly with the use of the local inventory compared to the results obtained using the global inventory. The LE-EDGAR simulation consistently underestimated the concentrations of $PM_{2.5}$ in all the stations analyzed (Figure 9, and Figure 13 (d) and (j)). The MFB values reported for LE-EDGAR in the *Normal Concentration Period* (Figure 13 (d)) remain around -1.0 and -1.2, and for the *High Concentration*

(a) Station 11 Normal Concentration Period.

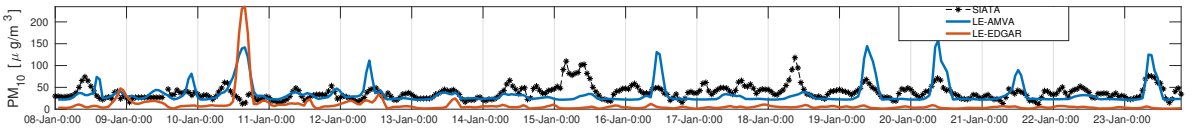


(b) Station 74 Normal Concentration Period.

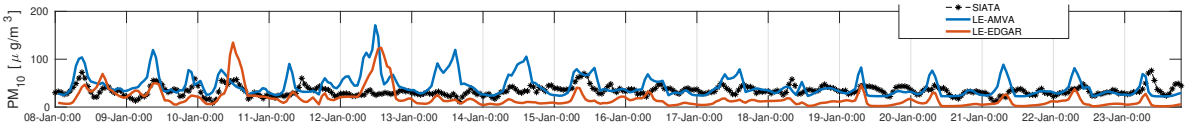


(c) Station 6 Normal Concentration Period.

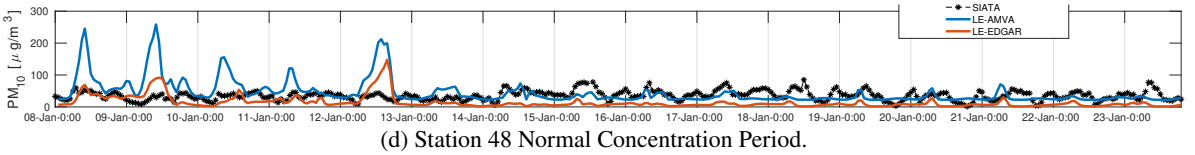


(d) Station 48 Normal Concentration Period.

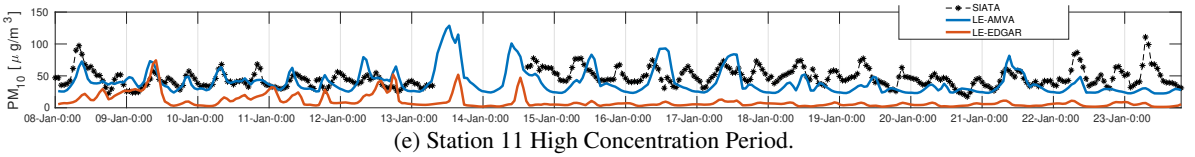


(e) Station 11 High Concentration Period.

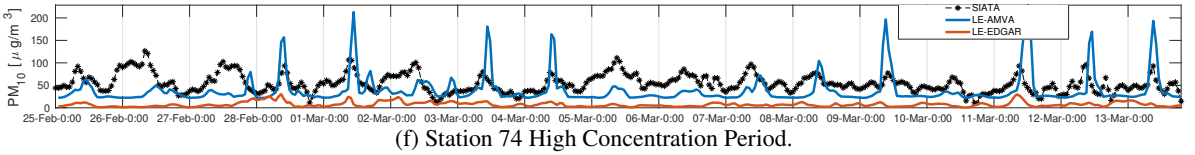


(f) Station 74 High Concentration Period.

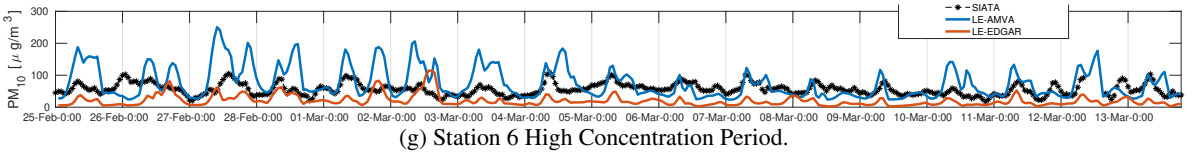


(g) Station 6 High Concentration Period.

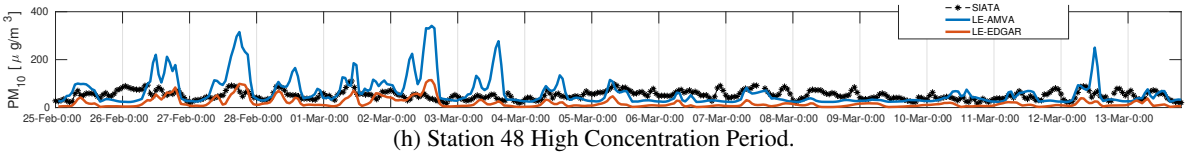


(h) Station 48 High Concentration Period.

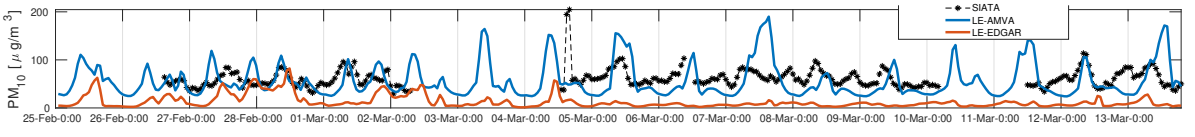


**Figure 10:** Comparison of LE-AMVA and LE-EDGAR $PM_{10}$ concentration against SIATA observations for both concentrations period. The time axis corresponds with the local time zone UTC-5.

*Period* between -1.3 and -1.6 (Figure 13 (j)). However, LE-AMVA simulations provided concentrations much closer to the observations (Figure 9, and Figure 13 (a) and (g)). An underestimation is often still present, but much reduced compared to LE-EDGAR, and in some cases concentrations are even higher than observed. The LE-AMVA simulation provides MFB values between -0.1 and 0.1 in the normal concentration period (Figure 13 (a)) and between -0.1 and -0.3 in the high concentration period (Figure 13 (g)). Underestimations are therefore larger during the high concentration period. This could be explained from poor meteorological representations of the conditions that caused the increase

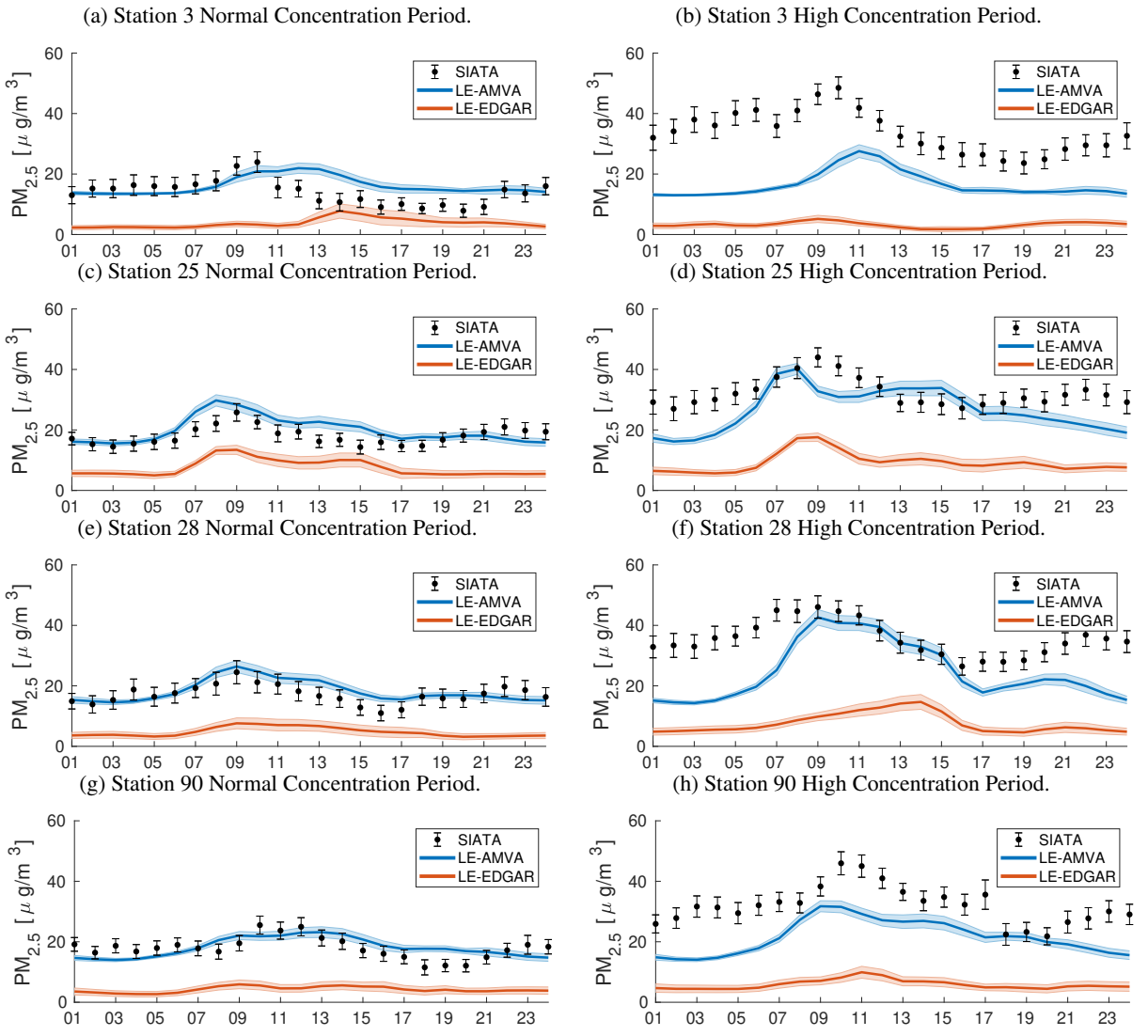


**Figure 11:** Comparison of LE-AMVA and LE-EDGAR $PM_{2.5}$ daily cycle against SIATA observations for both concentrations period. The time axis corresponds with the local time zone UTC-5.

in pollutant levels inside the valley, such as a low boundary layer height, high cloudiness, and increased atmospheric stability ((Herrera-Mejía and Hoyos, 2019; Roldán-Henao, Hoyos, Herrera-Mejía and Isaza, 2020)).

Representation of the temporal variability in $PM_{2.5}$ concentrations improved when the local inventory was used. RMSE values were lower for LE-AMVA than for LE-EDGAR (Figure 13 (b), (e), (h), and (k)), and like the MFB, they were higher in the high concentration period for both cases. Both configurations represented the diurnal variability rather accurate, with LE-AMVA simulations approaching the observations more closely than LE-EDGAR. During the *normal concentration period* the LE-AMVA simulations captured the highest peak in concentrations at around 09:00 (Figure 11 (a), (c), (e), and (g)), with a slight overestimation of the concentration between 11:00 and 17:00. During the *high concentration period* (Figure 11 (b), (d), (f), and (h)), pollutants remain trapped in the valley due to the high atmospheric stability, which generates higher concentrations in the afternoon Henao, Mejía, Rendón and Salazar (2020), the reason why LE-AMVA reproduces better this temporal variability (although not in terms of magnitude). While both LE-AMVA and LE-EDGAR are able to capture the daily cycle, the correlation factors CF shown in Figure 13 are lower than 0.5 what is usually declared as needed for good correlation (Chang and Hanna, 2004; Shaocai, Brian, Robin, Shao-Hang and E., 2006; Boylan and Russell, 2006). The low CF values arise because the representation of the

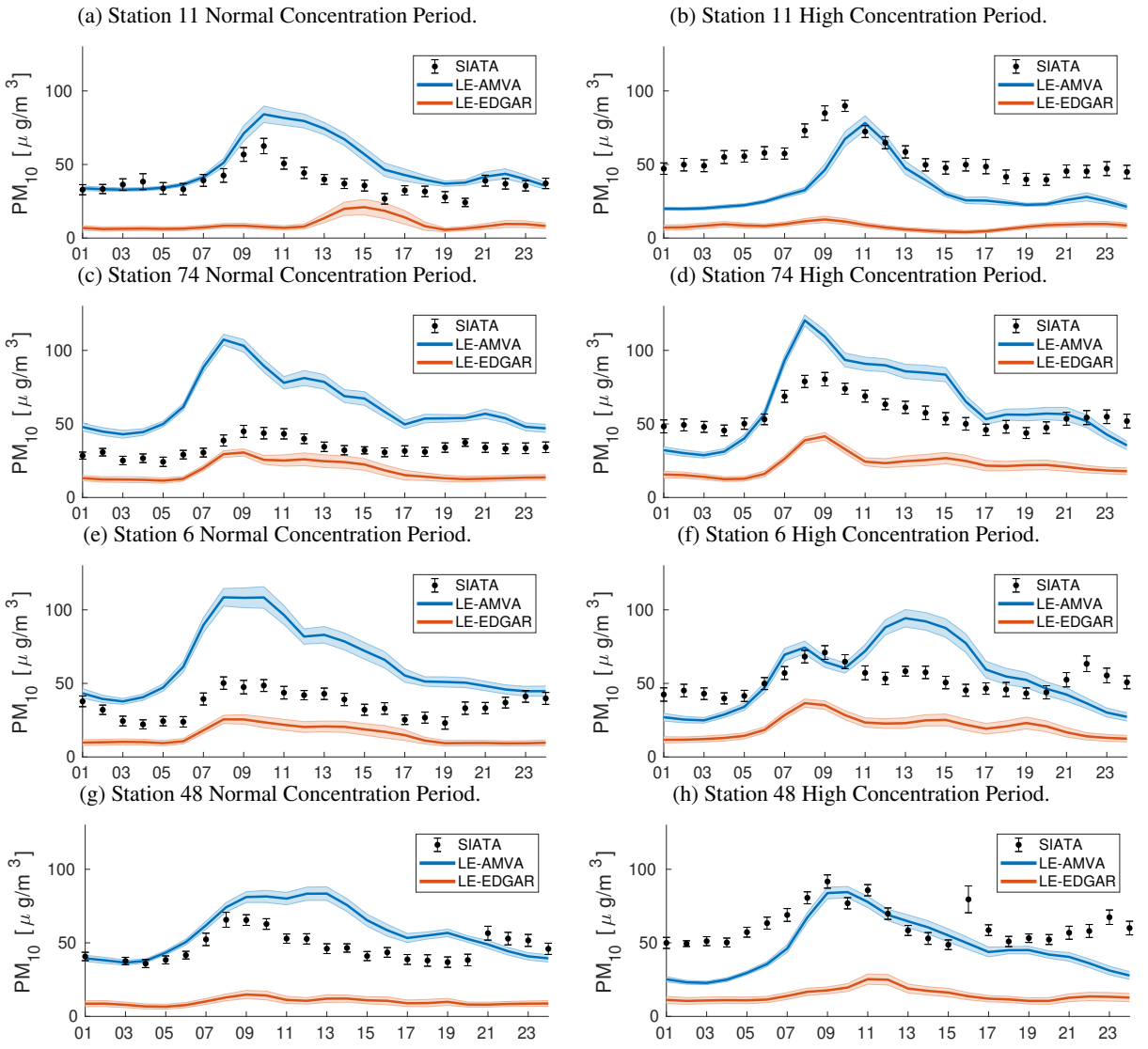


**Figure 12:** Comparison of LE-AMVA and LE-EDGAR $PM_{10}$ daily cycle against SIATA observations for both concentrations period. The time axis corresponds with the local time zone UTC-5.

day-to-day or long term variability model is less accurate. In spite of this, the CF values for LE-AMVA are higher than for LE-EDGAR. For both inventories, there is a higher correlation in the high concentration period, possibly generated by the better representation of the daily cycle mentioned above.

Similar to $PM_{2.5}$, LE-AMVA represents $PM_{10}$ better than LE-EDGAR. The temporal behavior of $PM_{10}$ is similar to that of $PM_{2.5}$. Both LE-AMVA and LE-EDGAR captured essential patterns of the $PM_{10}$ day cycle in the two simulated periods, such as the peak of the highest concentration around 09:00 and the low levels at night (Figure 12). The CF values improved with the use of the AMVA inventory, presenting higher values than for $PM_{2.5}$ (compare figures 13 and 14). The day-to-day variability was better captured for $PM_{10}$ than for $PM_{2.5}$. In terms of magnitude, LE-EDGAR underestimated $PM_{10}$ levels (Figures 10, 12 and 14 (d), (j)). Similar results were reported in (Kumar et al., 2016; González et al., 2018)) for Bogotá and Manizales. On the other hand, in some cases the LE-AMVA simulated $PM_{10}$ concentrations are much higher than the observations (Figures 10, 12 and 14 (a), (g)), which suggest an overestimation in the $PM_{10}$ emissions reported by AMVA. This is likely to originate from the industrial sector, which represents about 80 % of total $PM_{10}$ emissions (see Figure 2). As expected, the overestimation of $PM_{10}$ levels is smaller in the period of high concentrations due to the increase in the observed value.

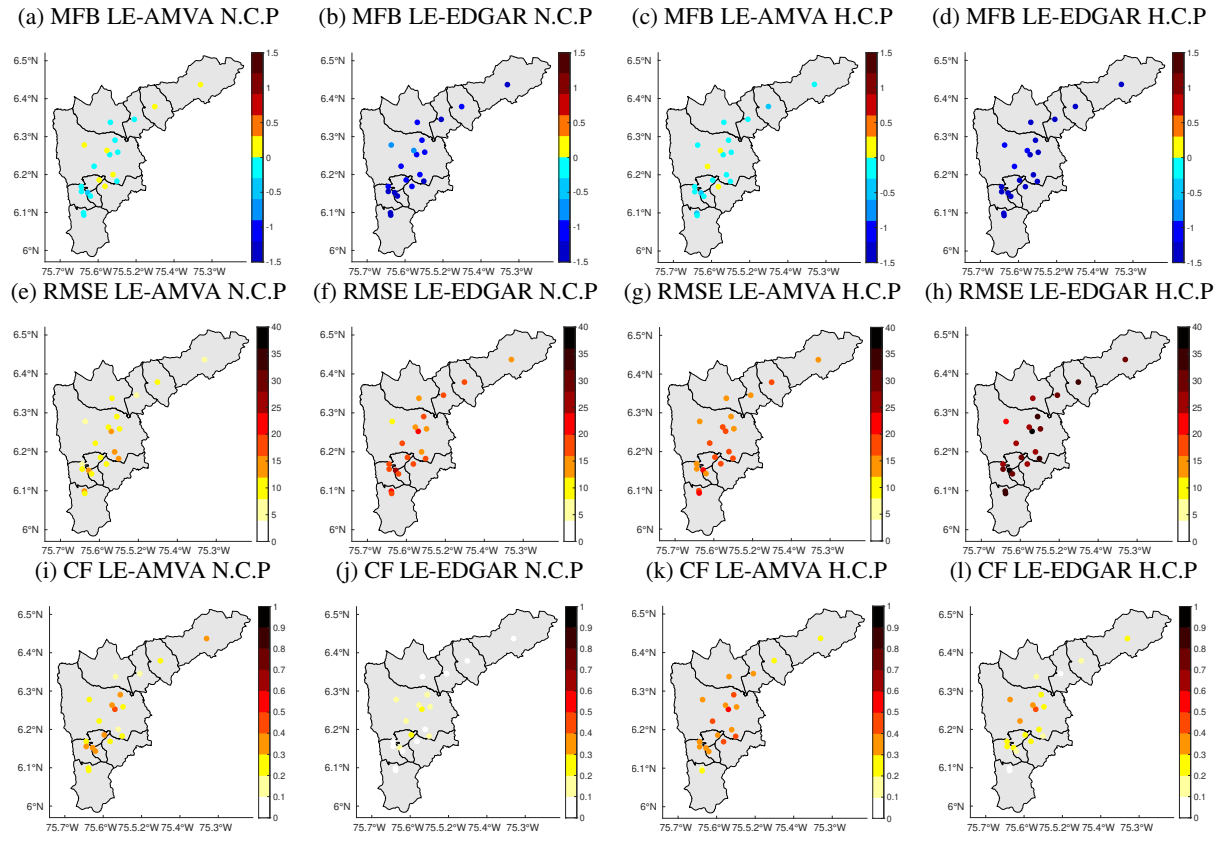


**Figure 13:** Statistical evaluation of the LOTOS-EUROS model using EDGAR v4.3 and AMVA inventory. The performance metrics were calculated over the 19 stations of $PM_{2.5}$ with enough data available for both periods shown in Figure 5. N.C.P and H.C.P refer to Normal and High Concentration Period respectively.

### 3.4. Simulated PM spatial distribution

Figure 15 shows maps of $PM_{2.5}$ concentrations averaged over the simulated periods. Similar figures for $PM_{10}$ are omitted since these are highly similar to the $PM_{2.5}$ results, while also the greater density of the $PM_{2.5}$ monitoring network (21 monitoring stations versus 9 for $PM_{10}$) makes an analysis for $PM_{2.5}$ most useful. A strongly improved spatial resolution has been obtained using the LE-AMVA simulations due to the higher spatial accuracy in positioning of point-source and road emissions. As mentioned above, EDGAR placed emissions hot-spots in the center and west of Medellin in mostly rural areas. Figures 15 (b) and (d) show the highest concentrations in these areas, which does not correspond to the values measured by the SIATA station located there (station 85 see Figure 5). Figures 15 (a) and (c) show that LE-AMVA obtained a better spatial representation, with the highest concentrations located in the center of the city of Medellin and around its main roads, in accordance with observations. In spite this, some significant discrepancies still appear, especially in the southern part of the metropolitan area. Stations 31 and 69 (Figure 5) present much higher values than those reported by LE-AMVA for the same locations in both simulated periods.

## 4. Conclusions

A spatial and temporal disaggregation of the official particulate matter emission inventory of the Metropolitan Area of the Aburrá Valley has been created. The spatial domain of this new AMVA inventory is centered over the Aburrá Valley at a high resolution of 1 km × 1 km.

The emission distribution factors for traffic emissions were calculated using a top-down methodology based on the road density, since actual traffic intensities are hardly available. For industrial point sources, actual locations are used. The higher resolution has led to a more detailed spatial representation of emissions. Despite the simple methodology, the AMVA inventory represents accurately the known hot-spots and high emissions regions for both on-road and point-

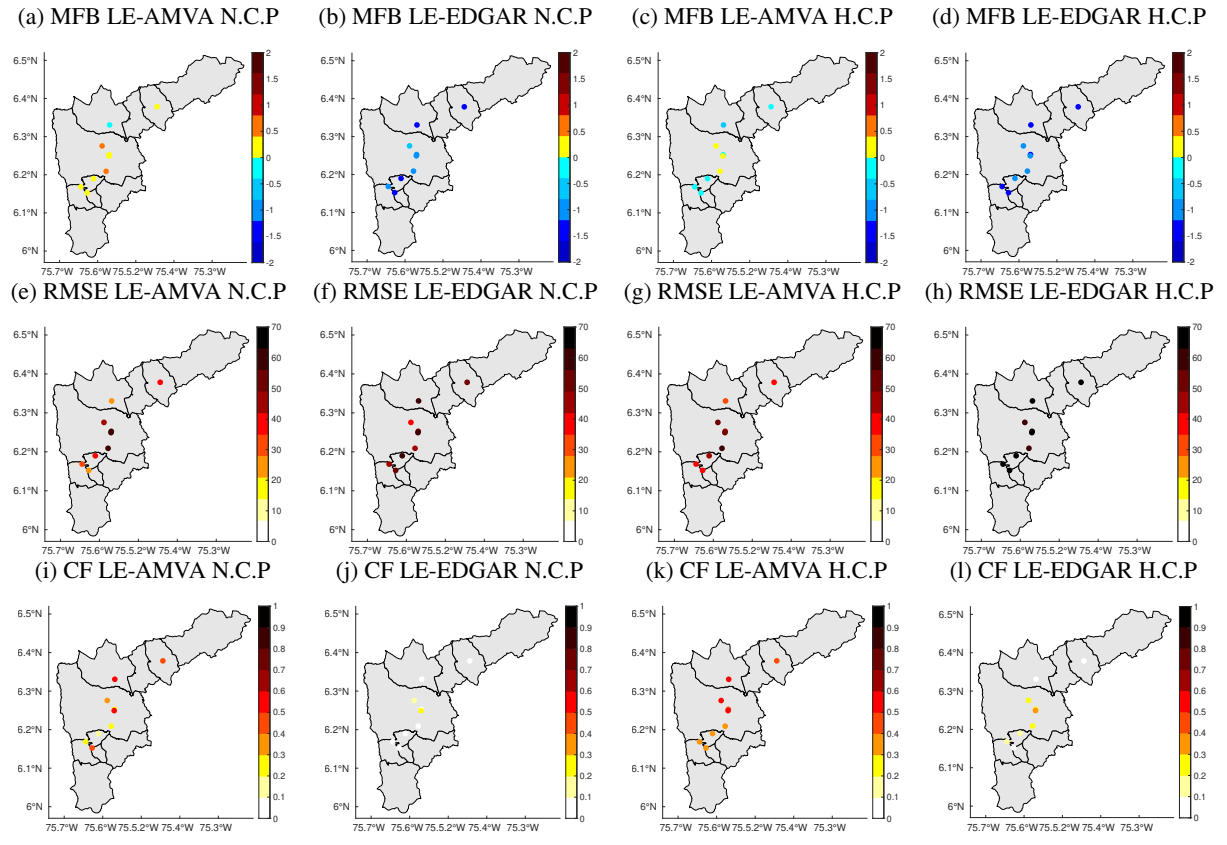


**Figure 14:** Statistical evaluation of the LOTOS-EUROS model using EDGAR V4.3 and AMVA inventory. The performance metrics were calculated over the 9 stations of $PM_{10}$ with enough data available for both periods shown in Figure 5. N.C.P and H.C.P correspond with normal and high concentration period respectively.

source industrial emissions.

Simulations with the LOTOS-EUROS model were performed using the both the global emission inventory EDGAR v4.3 and the new AMVA inventory, validating the results against the SIATA sensor network. The model simulations were evaluated in two different scenarios, a period of normal or average concentrations and a period of high concentrations. The simulated concentrations of $PM_{10}$ and $PM_{2.5}$ showed strongly improved representation of observations when the AMVA inventory was used. Particulate matter simulations were closer to observations with the AMVA inventory, reducing Mean-Fractional-Bias (MFB) and Root Mean Square Error (RMSE) during both episodes. The correlation between the modelled concentrations and the observations increased with the new emissions inventory for both size ranges and scenarios.

The results highlight the importance of detailed emissions information in regions where the global inventories are not accurate, as is the case for Colombia. Even simple methodologies as the one employed here could strengthen the capacity to represent and understand the dynamical behaviour of air pollution in complex cities.

An interesting future work, which is outside the scope of this paper, would be to implement data assimilation techniques to improve the model performance and correct model uncertainties in the emissions inventory and meteorological fields. The new high-resolution disaggregated AMVA inventory will support ongoing efforts to quantify exposure to air pollution in Medellín and surrounding area.

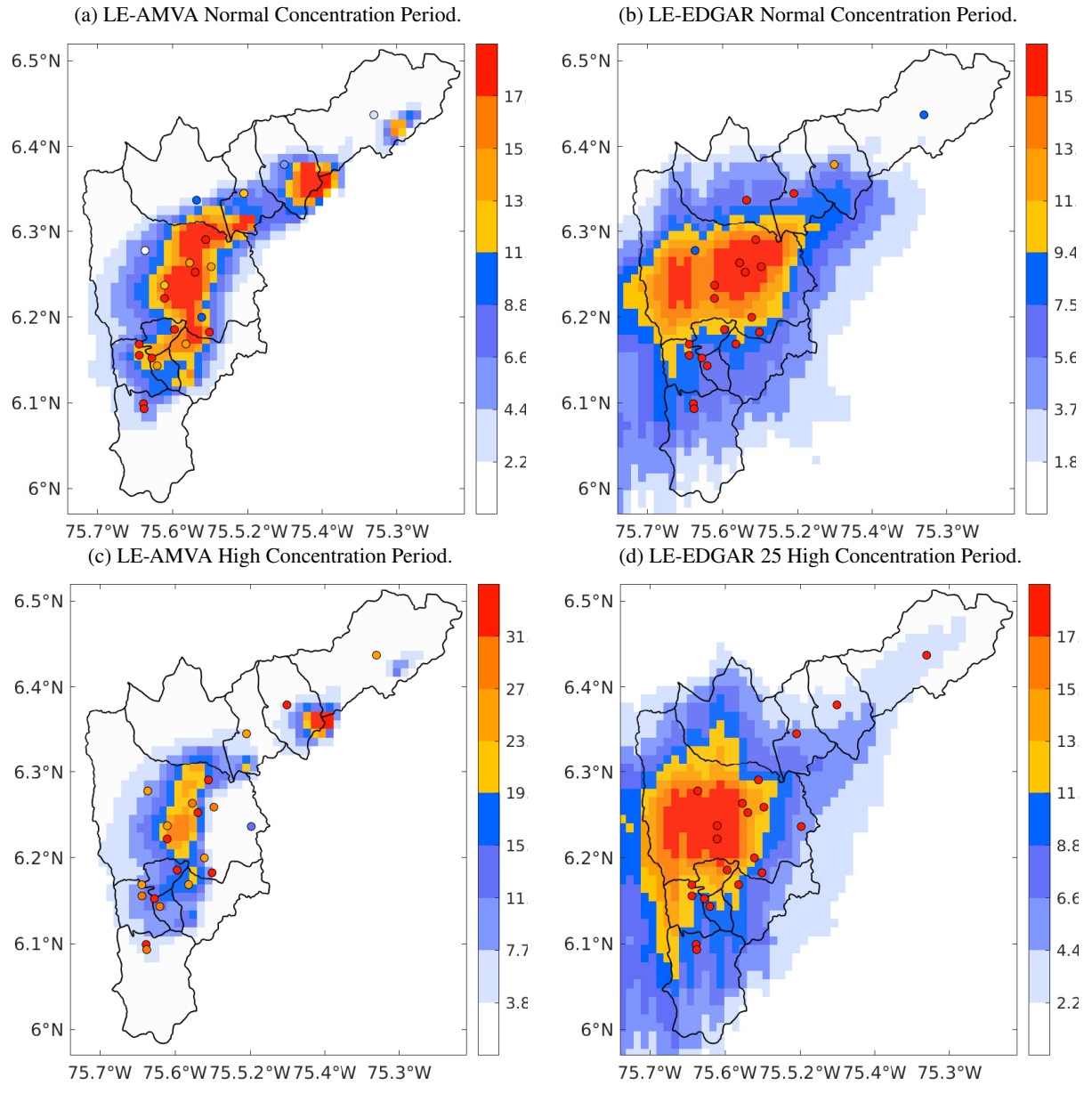


**Figure 15:** Comparison of LE-AMVA and LE-EDGAR $PM_{2.5}$ simulations averaged over periods of simulation. The circles represent the SIATA stations. The color scales are different to distinguish the spatial dynamics of each model simulation.

## CRediT authorship contribution statement

**Santiago Lopez-Restrepo:** Conceptualization, Methodology, Software, Writing - Original Draft. **Andres Yarce:** Methodology, Software. **Nicolás Pinel:** Conceptualization, Methodology, Writing - Review & Editing. **O. L. Quintero:** Conceptualization, Methodology, Writing - Original Draft- Review & Editing, Supervision. **Arjo Segers:** Methodology, Software, Writing - Review & Editing. **A. W. Heemink:** Writing - Review & Editing, Supervision.

## References

Boylan, J.W., Russell, A.G., 2006. Pm and light extinction model performance metrics, goals, and criteria for three-dimensional air quality models. Atmospheric Environment 40, 4946 – 4959. doi:https://doi.org/10.1016/j.atmosenv.2005.09.087. special issue on Model Evaluation: Evaluation of Urban and Regional Eulerian Air Quality Models.

Chai, T., Draxler, R.R., 2014. Root mean square error (rmse) or mean absolute error (mae): Arguments against avoiding rmse in the literature. Geoscientific Model Development 7, 1247–1250. doi:10.5194/gmd-7-1247-2014.

Chang, J.C., Hanna, S.R., 2004. Air quality model performance evaluation. Meteorology and Atmospheric Physics 87, 167–196. doi:10.1007/s00703-003-0070-7.

Crippa, M., Guizzardi, D., Muntean, M., Schaaf, E., Dentener, F., van Aardenne, J.A., Monni, S., Doering, U., Olivier, J.G.J., Pagliari, V., Janssens-Maenhout, G., 2018. Gridded emissions of air pollutants for the period 1970–2012 within edgar v4.3.2. Earth System Science Data 10, 1987–2013. URL: https://www.earth-syst-sci-data.net/10/1987/2018/, doi:10.5194/essd-10-1987-2018.

Curier, R.L., Timmermans, R., Calabretta-Jongen, S., Eskes, H., Segers, A., Swart, D., Schaap, M., 2012. Improving ozone forecasts over Europe by synergistic use of the LOTOS-EUROS chemical transport model and in-situ measurements. Atmospheric Environment 60, 217–226. doi:10.1016/j.atmosenv.2012.06.017.

Ferm, M., Sjöberg, K., 2015. Concentrations and emission factors for PM2.5 and PM10 from road traffic in Sweden. Atmospheric Environment 119, 211–219. doi:10.1016/j.atmosenv.2015.08.037.

Fu, G., Heemink, A., Lu, S., Segers, A., Weber, K., Lin, H.X., 2016. Model-based aviation advice on distal volcanic ash clouds by assimilating aircraft in situ measurements. Atmospheric Chemistry and Physics 16, 9189–9200. doi:10.5194/acp-16-9189-2016.

Gómez, C.D., González, C.M., Osses, M., Aristizábal, B.H., 2018. Spatial and temporal disaggregation of the on-road vehicle emission inventory in a medium-sized Andean city. Comparison of GIS-based top-down methodologies. Atmospheric Environment 179, 142–155. URL: https://doi.org/10.1016/j.atmosenv.2018.01.049, doi:10.1016/j.atmosenv.2018.01.049.

Gonzalez, C.M., Gomez, C.D., Rojas, N.Y., Acevedo, H., Aristizabal, B.H., 2017. Relative impact of on-road vehicular and point-source industrial emissions of air pollutants in a medium-sized Andean city. Atmospheric Environment 152, 279–289. doi:10.1016/j.atmosenv.2016.12.048.

González, C.M., Ynoue, R.Y., Vara-Vela, A., Rojas, N.Y., Aristizábal, B.H., 2018. High-resolution air quality modeling in a medium-sized city in the tropical Andes: Assessment of local and global emissions in understanding ozone and PM10 dynamics. Atmospheric Pollution Research , 1–15doi:10.1016/j.apr.2018.03.003.

Green, J., Sánchez, S., 2012. Air Quality in Latin America: An Overview. Technical Report. Clean air Institute. Washington D.C., USA. doi:10.1017/CBO9781107415324.004.

Haklay, M., Weber, P., 2008. Openstreetmap: User-generated street maps. IEEE Pervasive Computing 7, 12–18.

Henao, J.J., Mejía, J.F., Rendón, A.M., Salazar, J.F., 2020. Sub-kilometer dispersion simulation of a co tracer for an inter-andean urban valley. Atmospheric Pollution Research 11, 928 – 945. doi:https://doi.org/10.1016/j.apr.2020.02.005.

Herrera-Mejía, L., Hoyos, C.D., 2019. Characterization of the atmospheric boundary layer in a narrow tropical valley using remote-sensing and radiosonde observations and the wrf model: the aburrá valley case-study. Quarterly Journal of the Royal Meteorological Society 145, 2641–2665. URL: https://rmets.onlinelibrary.wiley.com/doi/abs/10.1002/qj.3583, doi:10.1002/qj.3583, arXiv:https://rmets.onlinelibrary.wiley.com/doi/pdf/10.1002/qj.3583.

Hoyos, C.D., Herrera-Mejía, L., Roldán-Henao, N., Isaza, A., 2019. Effects of fireworks on particulate matter concentration in a narrow valley: the case of the medellín metropolitan area. Environmental Monitoring and Assessment 192, 6. URL: https://doi.org/10.1007/s10661-019-7838-9, doi:10.1007/s10661-019-7838-9.

Jiménez, J.F., 2016. Altura de la Capa de Mezcla en un área urbana montañosa y tropical. Caso de estudio: Valle de Aburrá (Colombia). Doctoral thesis. Universidad de Antioquia. Medellín.

Jin, J., Lin, H.X., Heemink, A., Segers, A., 2018. Spatially varying parameter estimation for dust emissions using reduced-tangent-linearization 4DVar. Atmospheric Environment doi:10.1016/j.atmosenv.2018.05.060.

Kumar, A., Jiménez, R., Belalcázar, L.C., Rojas, N.Y., 2016. Application of WRF-Chem Model to Simulate PM10 Concentration over Bogota. Aerosol and Air Quality Research 16, 1206–1221. doi:10.4209/aaqr.2015.05.0318.

Lateb, M., Meroney, R., Yataghene, M., Fellouah, H., Saleh, F., Boufadel, M., 2016. On the use of numerical modelling for near-field pollutant dispersion in urban environments: A review. Environmental Pollution 208, 271–283. doi:10.1016/j.envpol.2015.07.039.

Lopez-Restrepo, S., Yarce, A., Pinel, N., Quintero, O., Segers, A., Heemink, A., 2020. Forecasting $PM_{10}$ and $PM_{2.5}$ in the Aburrá Valley (Medellín, Colombia) via EnKF based Data Assimilation. Atmospheric Environment , . doi:10.1016/j.atmosenv.2020.117507.

Manders, A.M., Schaap, M., Hoogerbrugge, R., 2009. Testing the capability of the chemistry transport model LOTOS-EUROS to forecast PM10 levels in the Netherlands. Atmospheric Environment 43, 4050–4059. doi:10.1016/j.atmosenv.2009.05.006.

Manders, A.M.M., Builtjes, P.J.H., Curier, L., Denier Van Der Gon, H.A.C., Hendriks, C., Jonkers, S., Kranenburg, R., Kuenen, J.J.P., Segers, A.J., Timmermans, R.M.A., Visschedijk, A.J.H., Kruit, R.J.W., Addo, W., Van Pul, J., Sauter, F.J., Van Der Swaluw, E., Swart, D.P.J., Douros, J., Eskes, H., Van Meijgaard, E., Van Ulft, B., Van Velthoven, P., Banzhaf, S., Mues, A.C., Stern, R., Fu, G., Lu, S., Heemink, A., Van Velzen, N., Schaap, M., 2017. Curriculum vitae of the LOTOS–EUROS (v2.0) chemistry transport model. Geosci. Model Dev 10, 4145–4173. doi:10.5194/gmd-10-4145-2017.

Mues, a., Kuenen, J., Hendriks, C., Manders, a., Segers, a., Scholz, Y., Hueglin, C., Builtjes, P., Schaap, M., 2014. Sensitivity of air pollution simulations with LOTOS-EUROS to the temporal distribution of anthropogenic emissions. Atmospheric Chemistry and Physics 14, 939–955. doi:10.5194/acp-14-939-2014.

Nedbor-Gross, R., Henderson, B.H., Pérez-Peña, M.P., Pachón, J.E., 2018. Air quality modeling in Bogotá Colombia using local emissions and natural mitigation factor adjustment for re-suspended particulate matter. Atmospheric Pollution Research 9, 95–104. doi:10.1016/j.apr.2017.07.004.

Ossés de Eicker, M., Zah, R., Triviño, R., Hurni, H., 2008. Spatial accuracy of a simplified disaggregation method for traffic emissions applied in seven mid-sized Chilean cities. Atmospheric Environment 42, 1491–1502. doi:10.1016/j.atmosenv.2007.10.079.

Pachón, J.E., Galvis, B., Lombana, O., Carmona, L.G., Fajardo, S., Rincón, A., Meneses, S., Chaparro, R., Nedbor-Gross, R., Henderson, B., 2018. Development and evaluation of a comprehensive atmospheric emission inventory for air quality modeling in the megacity of Bogotá. Atmosphere 9, 1–17. doi:10.3390/atmos9020049.

Premalatha Kanikannan, R., Duraiswamy, K., 2014. Face recognition system based on spectral graph wavelet theory. Research Journal of Applied Sciences, Engineering and Technology 8, 1456–1460. doi:10.19026/rjaset.8.1121.

Roldán-Henao, N., Hoyos, C.D., Herrera-Mejía, L., Isaza, A., 2020. An investigation of the precipitation net effect on the particulate matter concentration in a narrow valley: Role of lower-troposphere stability. Journal of Applied Meteorology and Climatology 59, 401–426. doi:10.1175/JAMC-D-18-0313.1.

Saide, P., Zah, R., Osses, M., Ossés de Eicker, M., 2009. Spatial disaggregation of traffic emission inventories in large cities using simplified top-down methods. Atmospheric Environment 43, 4914–4923. URL: http://dx.doi.org/10.1016/j.atmosenv.2009.07.013, doi:10.1016/j.atmosenv.2009.07.013.

Sauter, F., der Swaluw, E.V., Manders-groot, A., Kruit, R.W., Segers, A., Eskes, H., 2012. TNO report TNO-060-UT-2012-01451. Technical Report. TNO. Utrecht, Netherlands.

Shaocai, Y., Brian, E., Robin, D., Shao-Hang, C., E., S.S., 2006. New unbiased symmetric metrics for evaluation of air quality models. Atmospheric Science Letters 7, 26–34. doi:10.1002/asl.125.

Shu, Y., Lam Nina, N.S.N., 2011. Spatial disaggregation of carbon dioxide emissions from road traffic based on multiple linear regression model. Atmospheric Environment 45, 634–640. URL: http://dx.doi.org/10.1016/j.atmosenv.2010.10.037, doi:10.1016/j.atmosenv.2010.10.037.

Thunis, P., Miranda, A., Baldasano, J.M., Blond, N., Douros, J., Graff, A., Janssen, S., Juda-Rezler, K., Karvosenoja, N., Maffeis, G., Martilli, A., Rasoloharimahefa, M., Real, E., Viaene, P., Volta, M., White, L., 2016. Overview of current regional and local scale air quality modelling practices: Assessment and planning tools in the EU. Environmental Science & Policy 65, 13–21. doi:10.1016/j.envsci.2016.03.013.

Tuia, D., Ossés de Eicker, M., Zah, R., Osses, M., Zarate, E., Clappier, A., 2007. Evaluation of a simplified top-down model for the spatial assessment of hot traffic emissions in mid-sized cities. Atmospheric Environment 41, 3658–3671. doi:10.1016/j.atmosenv.2006.12.045.

UPB, AMVA, 2017. Inventario de Emisiones Atmosféricas del Valle de Aburrá - actualización 2015. Technical Report. Universidad Pontificia Bolivariana - Grupo de Investigaciones Ambientales, Area Metropolitana del Valle de Aburra. Medellín. URL: https://www.metropol.gov.co/ambiental/calidad-del-aire/Documents/Inventario-de-emisiones.

US EPA (United State Environmental Protection Agency), 1995. AP-42: Compilation of Air Emissions Factors. Technical Report. US EPA (United State Environmental Protection Agency). URL: https://www.epa.gov/air-emissions-factors-and-quantification/ap-42-compilation-air-emissions-factors.

Zavala, M., Barrera, H., Morante, J., Molina, L.T., 2013. Analysis of model-based PM2.5 emission factors for on-road mobile sources in Mexico. Atmosfera 26, 109–124. doi:10.1016/S0187-6236(13)71065-8.

Zhang, S., Roussel, N., Boniface, K., Cuong Ha, M., Frappart, F., Darrozes, J., Baup, F., Calvet, J.C., 2017. Use of reflected GNSS SNR data to retrieve either soil moisture or vegetation height from a wheat crop. Hydrology and Earth System Sciences 21, 4767–4784. doi:10.5194/hess-21-4767-2017.